Fermionic-bosonic couplings in a weakly deformed odd-mass nucleus, $^{93}_{41}$Nb

J. N. Orce,[1,2,*] J. D. Holt,[2,3,4] A. Linnemann,[5] C. J. McKay,[1] C. Fransen,[5] J. Jolie,[5] T. T. S. Kuo,[6] S. R. Lesher,[1,7] M. T. McEllistrem,[1] N. Pietralla,[5,8] N. Warr,[5] V. Werner,[5,9] and S. W. Yates[1,10]

[1]*Department of Physics and Astronomy, University of Kentucky, Lexington, Kentucky 40506-0055, USA*
[2]*TRIUMF, 4004 Wesbrook Mall, Vancouver, BC V6T 2A3, Canada*
[3]*Physics Division, Oak Ridge National Laboratory, P. O. Box 2008, Oak Ridge, Tennessee 37831, USA*
[4]*Department of Physics and Astronomy, University of Tennessee, Knoxville, Tennessee 37996, USA*
[5]*Institut für Kernphysik, Universität zu Köln, D-50937 Köln, Germany*
[6]*Department of Physics and Astronomy, Nuclear Structure Laboratory, SUNY, Stony Brook, New York 11794-3800, USA*
[7]*Department of Physics, University of Wisconsin-La Crosse, 1725 State Street, La Crosse, Wisconsin 54601, USA*
[8]*Institut für Kernphysik, Technische Universität Darmstadt, D-64289 Darmstadt, Germany*
[9]*Wright Nuclear Structure Laboratory, Yale University, New Haven, Connecticut 06520-8120, USA*
[10]*Department of Chemistry, University of Kentucky, Lexington, Kentucky 40506-0055, USA*

(Received 15 July 2010; revised manuscript received 13 September 2010; published 25 October 2010)

A comprehensive level scheme of ^{93}Nb below 2 MeV has been constructed from information obtained with the ^{93}Nb$(n,n'\gamma)$ and the ^{94}Zr$(p,2n\gamma\gamma)^{93}$Nb reactions. Branching ratios, lifetimes, transition multipolarities, and spin assignments have been determined. From $M1$ and $E2$ strengths, fermionic-bosonic excitations of isoscalar and isovector characters have been identified from the weak couplings of the $\pi 1g_{9/2} \otimes {}^{92}_{40}$Zr and $\pi 2p^{-1}_{1/2} \otimes {}^{94}_{42}$Mo configurations. A microscopic interpretation of such excitations is obtained from shell-model calculations, which use low-momentum effective interactions.

DOI: 10.1103/PhysRevC.82.044317 PACS number(s): 21.10.Tg, 23.20.Js, 25.40.−h, 27.60.+j

I. INTRODUCTION

The low-lying structure of an odd-A nucleus can generally be described in terms of a valence nucleon coupled to the excited states of the neighboring even-even core [1–3]. In the weak-coupling limit, the coupling Hamiltonian can be treated as a perturbation, whereas intermediate coupling also allows for mixing between several single-particle states coupled to core excitations. The angular momentum of the core $J_{\rm core}$ and single-particle (or particle-hole) states $J_{\rm sp}$ couple to form a multiplet of states with a total angular momentum [4–8] given by

$$|J_{\rm sp} - J_{\rm core}| \leqslant J_{\rm core} \otimes J_{\rm sp} \leqslant |J_{\rm sp} + J_{\rm core}|. \quad (1)$$

In fact, low-lying excited states in ^{93}Nb can be regarded as resulting from the coupling of a $1g_{9/2}$ proton to a $^{92}_{40}$Zr core and a $2p^{-1}_{1/2}$ proton-hole to a $^{94}_{42}$Mo core [8]. These couplings result in two independent and unmixed one-phonon structures of opposite parities: (a) a quintet of positive-parity states built on the $J^\pi = 9/2^+_1$ ground state, which results from the $\pi 1g_{9/2} \otimes (2^+_1, {}^{92}$Zr) coupling; and (b) a pair of negative-parity states built on the isomeric $J^\pi = 1/2^-_1$ state (with a half-life of 16 years) at 31 keV above the ground state, which corresponds to the $\pi 2p^{-1}_{1/2} \otimes (2^+_1, {}^{94}$Mo) configuration.

Low-lying collective excitations in weakly deformed odd-mass nuclei have rarely been studied in detail because of the structural complexity, which arises from the interplay of various single-particle excitations and collective degrees of freedom. With increasing angular momentum for the ground and single-particle states, bountiful excitations and a distribution of strength among several levels occur; however, the weak coupling of a single particle to the bosonic core would provide structural simplifications. Such a scenario is present in the low-energy structure of the weakly deformed odd-mass nucleus $^{93}_{41}$Nb$_{52}$, with $Q_s(9/2^+_1) = -0.32(2)b$ [9], which exhibits unique and nearly unmixed structures below 2 MeV built on the $\pi 1g_{9/2}$ ground state and the $\pi 2p^{-1}_{1/2}$ proton-hole excited state. These two separate structures are presented and are discussed according to the parity of the states and their isoscalar (*IS*) and isovector (*IV*) characters.

The magnetic dipole operator $\hat{M}1$ can be decomposed into *IS* and *IV* terms,

$$\begin{aligned}\hat{M}1 &= IS(\Delta T = 0) + IV(\Delta T = \pm 1)\\ &\propto \sum_{i=1}^{N,Z} \mu_N \left[\frac{1}{2}\left(g^s_\pi + g^s_\nu\right)\boldsymbol{s} + \left(g^l_\pi + g^l_\nu\right)\boldsymbol{\ell}\right]\\ &\quad + \sum_{i=1}^{N,Z} \mu_N \left[\frac{1}{2}\left(g^s_\pi - g^s_\nu\right)\boldsymbol{s} + \left(g^l_\pi - g^l_\nu\right)\boldsymbol{\ell}\right]\boldsymbol{\tau}_3, \quad (2)\end{aligned}$$

where $\boldsymbol{\ell}$, $\boldsymbol{s}$, and $\boldsymbol{\tau}_3$ are the orbital, the spin, and the z-component isospin operators, respectively, μ_N is the nuclear magneton and $g^l_\pi = 1\,\mu_N$, $g^l_\nu = 0$ and $g^s_\pi = 5.586\,\mu_N$, $g^s_\nu = -3.826\,\mu_N$ are the orbital and the spin proton and neutron g factors in free-nuclear matter, respectively. Collective *IV* excitations occur when nucleons and their spins are collectively excited, which leads to large $\langle i||\boldsymbol{s}||f\rangle$ matrix elements. In addition, proton and neutron spin g factors are additive in the vector part of the magnetic dipole ($\hat{M}1$) operator, which may lead to large $M1$ transition strengths. The scissors mode [10] in deformed nuclei [11–14] and mixed-symmetry (*MS*) states in weakly deformed even-even nuclei [15–18] are examples of collective

*jnorce@triumf.ca; URL: http://www.pa.uky.edu/∼jnorce

IV excitations. The latter was predicted by the algebraic interacting boson model-2 with separate representations for proton and neutron bosons [19] and interpreted as a collective motion of protons and neutrons not in phase. Such *IV* excitations have been widely observed in weakly deformed even-even nuclei [15]. Both *IS* and *IV* excitations have been identified in the negative-parity structure of ^{93}Nb built on the $2p_{1/2}^{-1}$ proton-hole excited state [20]. This paper provides a microscopic many-body interpretation of *IS* and *IV* excitations.

Mixed-symmetry states have been explained from a shell-model (*SM*) basis by Lisetskiy and collaborators [21] by using a surface δ interaction with tuned parameters. Large *IS* $E2$ matrix elements were found between states with *MS* assignments and were interpreted as excitations with similar *pn* symmetry. In a microscopic many-body framework, *SM* calculations, which use an ^{88}Sr core and effective low-momentum interactions $V_{\mathrm{low}\,k}$ [22] have successfully accounted for excitation energies, level densities, $M1$ and $E2$ transition strengths, *IS* and *IV* excitations, and both spin and orbital contributions to the $M1$ transition matrix elements in the negative-parity structure of ^{93}Nb [20]. As a successor to that work, we present a more extensive spectroscopic and microscopic study of ^{93}Nb, which includes both positive- and negative-parity structures.

II. EXPERIMENTAL DETAILS

The nucleus ^{93}Nb has been studied with the $(n,n'\gamma)$ reaction at the University of Kentucky and in a ^{94}Zr$(p,2n)^{93}$Nb γ-γ coincidence experiment at the University of Cologne.

A. ^{93}Nb$(n,n'\gamma)$ experiments

Excitation functions, lifetimes, and branching ratios were measured by using the ^{93}Nb$(n,n'\gamma)$ reaction [23] at neutron energies, which range from 1.5 to 2.6 MeV. Neutrons were provided by the 7-MV electrostatic accelerator at the University of Kentucky through the ^{3}H$(p,n)^{3}$He reaction. The scattering sample was 56 g of Nb, which is naturally monoisotopic, in a 3×2-cm cylinder. Pulsed-beam techniques were used to reduce background, with beam pulses separated by 533 ns and bunched to about 1 ns. The time-of-flight technique for background suppression was employed by gating on the appropriate prompt time windows [23]. Finally, γ rays were detected by using a BGO Compton-suppressed 55% HPGe spectrometer with 2.0-keV resolution. Both excitation functions and angular distributions were normalized to the neutron flux.

From the angular distribution experiments, lifetimes were determined through the Doppler-shift attenuation method, which followed the $(n,n'\gamma)$ reaction [24]. Here, the shifted γ-ray energy is given by

$$E_\gamma(\theta_\gamma) = E_{\gamma_0}\left[1 + \frac{v_0}{c}F(\tau)\cos\theta_\gamma\right], \qquad (3)$$

with E_{γ_0} as the unshifted γ-ray energy, v_0 as the initial recoil velocity in the center-of-mass frame, θ as the angle of observation, and $F(\tau)$ as the attenuation factor, which is related to the nuclear stopping process described by Blaugrund [25]. Finally, the lifetimes of the states can be determined by comparison with the $F(\tau)$ values calculated by using the Winterbon formalism [26].

Furthermore, γ-ray coincidences were observed through the $(n,n'\gamma\gamma)$ reaction at a neutron energy of 3 MeV to identify the decay paths of γ rays, to measure their branching ratios, and to confirm the results from the excitation functions. The coincidence methods have been described by McGrath *et al.* [27].

B. ^{94}Zr$(p,2n)^{93}$Nb angular-correlation experiment

For odd-mass nuclei, particularly those with high ground-state spins, the angular distributions of the photons from scattering reactions are rather isotropic, and the $(n,n'\gamma)$ data cannot generally be used for assigning the spins of excited states. Complementarily, from a γ-γ coincidence experiment with the ^{94}Zr$(p,2n\gamma\gamma)^{93}$Nb reaction, many multipolarities and spin assignments could be determined, and branching ratios were measured. The proton beam provided by the 10-MV tandem accelerator at the University of Cologne bombarded a 2-mg/cm^2-thick ^{94}Zr target enriched to 96.93% with beam currents from 2 to 3 nA. The proton energies were in the range of 11.5 to 19 MeV. The deexciting γ rays were detected by using the HORUS spectrometer [28], composed of 16 HPGe detectors with the following features: (a) Seven of the detectors formed a EUROBALL cluster detector [29] with the central detector placed at $\theta = 90^\circ$ with respect to the beam axis and $\phi = 0^\circ$, where ϕ is the clockwise angle around the beam axis; (b) four detectors placed at $\theta = 45^\circ$ and 135° in a vertical plane above and below the beam axis were complemented by Compton-suppression shields; (c) the remaining detectors were placed in the $\theta = 90^\circ$ plane and at angles of $\phi = 55^\circ$, 125°, 235°, and 305°. Given the detector combinations, nine possible angular-correlation groups can be characterized by $(\theta_1, \theta_2, \phi)$ angles, where θ_1 and θ_2 are the angles of the two detector axes relative to the beam axis and the angle ϕ between the planes is defined by the beam axis and emission directions of the γ rays. Because of problems that concern the efficiency of the cluster detector, only seven out of the nine possible correlation groups were used for this analysis. When possible, we determined the $E2/M1$ mixing ratio $\delta^2 = \Gamma_{f,E2}/\Gamma_{f,M1}$ [30] by fitting the angular-correlation data as a function of angles, θ_1, θ_2, and ϕ, by following the formalism developed by Krane and Steffen [31]. The current results are in agreement with the most intense transitions identified in previous work [8,32]. As an example of this agreement, the top panel of Fig. 1 shows an angular-correlation plot for the previously known 338-keV γ ray, which depopulates the 1082-keV one-phonon excitation. A value of $\delta_{744} = 0.26(8)$ was fixed from the angular-correlation analysis of γ rays that populate the 744-keV level.

III. DATA ANALYSIS AND RESULTS

In a previous work by van Heerden and McMurray [8], angular momenta, parities, and transition rates for several

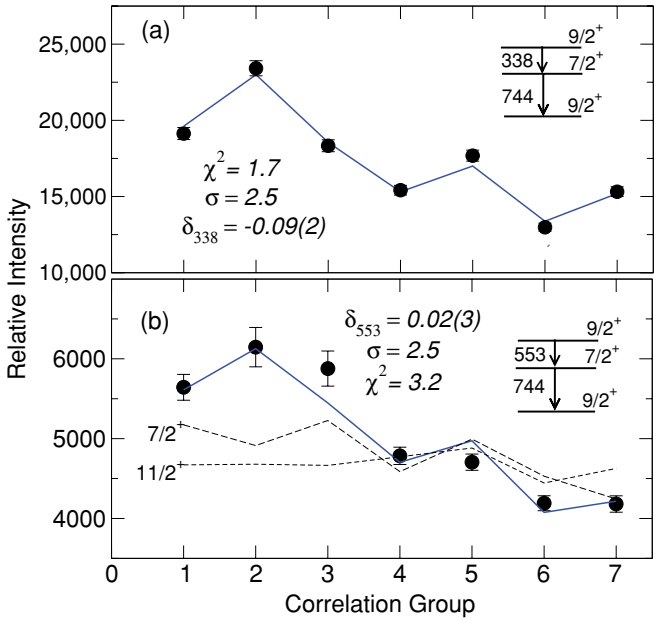

FIG. 1. (Color online) Angular-correlation plots for (a) the 338-keV and (b) the 553-keV transitions gated by the 744-keV γ ray. The fits to the data give mixing ratios of $\delta_{338} = -0.09(2)$ [in agreement with previous work $\delta_{338} = -0.12(5)$] and a more precise $\delta_{553} = 0.02(3)$ as compared with previous work $\delta = -0.3^{+3}_{-7}$ [33]. Dashed lines indicate other angular-correlation fits with unlikely spins for the 1297.4-keV level. The fitting parameter σ is the width of the magnetic substate distribution, usually found to be between 2 and 3.

of the first ten states (up to 1.1 MeV) were presented. The low-lying structure of ^{93}Nb is dominated by the $\pi 1g_{9/2}$ and $\pi 2p^{-1}_{1/2}$ single-particle and proton-hole excitations, respectively, and jj couplings built on these [8,32,34–36]. In particular, the $\pi 1g_{9/2}$ ground state couples to the 2^+_1 state of the ^{92}Zr core to give a quintet of *IS* excitations $J^\pi = 5/2^+_1$, $7/2^+_1$, $9/2^+_2$, $11/2^+_1$, and $13/2^+_1$. The $3/2^-_1$ and $5/2^-_1$ states are also identified as being built on the low-lying $\pi 2p^{-1}_{1/2}$ excitation. Our results are in agreement with previous work.

Excitation functions, together with the analysis of gated coincidence spectra, allowed the construction of a comprehensive level scheme up to 2.2 MeV. Figure 2 shows the total projection of the coincidence matrix built from the ^{93}Nb($n,n'\gamma\gamma$) experiment, with the main γ-ray transitions that depopulate the nucleus labeled. The data also support two well-defined and nearly separate structures as the main characteristic of this nucleus. Figure 3 shows typical background-subtracted spectra gated on the 744- and 780-keV transitions, which feed the ground state and the $1/2^-_1$ state, respectively, by indicating the different decay patterns as well as the quality of the data.

A. $\pi 1g_{9/2} \otimes (2^+_1, {}^{92}\mathrm{Zr})$ configuration

The $\pi 1g_{9/2} \otimes (2^+_1, {}^{92}\mathrm{Zr})$ configuration assignment is supported by the center-of-gravity theorem [4,8], which implies, through the j-j coupling shell model, the existence of

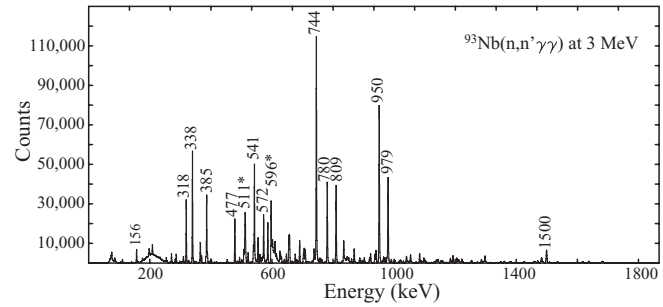

FIG. 2. Background-subtracted total projection of the γ-γ-coincidence matrix from the ^{93}Nb($n,n'\gamma\gamma$) reaction at an incident neutron energy of 3 MeV. The labeled transitions belong to ^{93}Nb, except for those indicated by asterisks (electron-positron annihilation and radiation produced by neutrons, which strike the HPGe detectors).

geometrical relations among the spectra of neighboring nuclei. The center-of-gravity energy of the one-phonon system ΔE_{CG} is then given by the relation,

$$(2j_p + 1)\Delta E_{\mathrm{CG}} = (2J_{\mathrm{core}} + 1)^{-1} \sum_{J_3} (2J_3 + 1)E_{J_3}, \quad (4)$$

where j_p is the angular momentum of the coupled particle (in our case $g_{9/2}$), J_{core} is the angular momentum of the core state (2^+), and J_3, E_{J_3} are the spins and excitation energies, respectively, of the single one-phonon states. By considering the first five excited positive-parity states in ^{93}Nb as one-phonon excitations and $Z = 40$ as a semiclosed shell for protons, the predicted center-of-gravity excitation energy is 934 keV. This energy is in striking agreement with the 934.5 keV measured for the first excited 2^+ state in ^{92}Zr [37,38]. In addition, from Coulomb excitation studies, the sum of $B(E2)\uparrow$ values for the quintet of one-phonon states proposed in ^{93}Nb, $765(11)e^2$ fm^4 (weighted average from Refs. [32,39–41]), matches the excitation of the 2^+ core state,

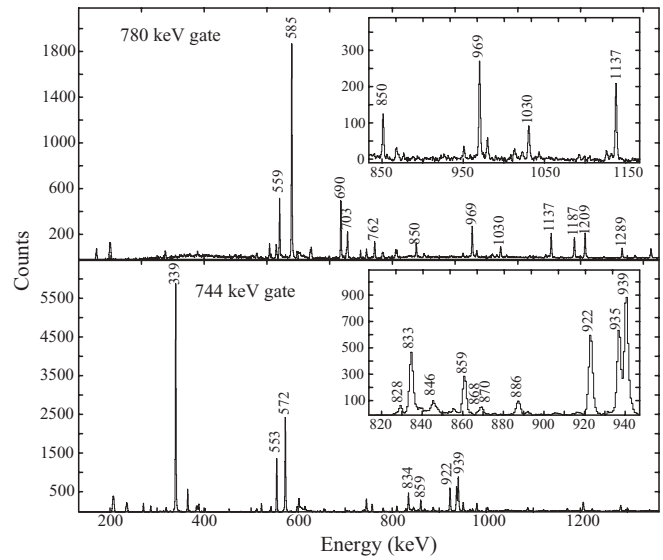

FIG. 3. Background-subtracted γ-ray spectra gated by the 744- and the 780-keV transitions in the ^{93}Nb($n,n'\gamma\gamma$) coincidence matrix.

795(56)e^2 fm^4 (weighted average from Refs. [39,42]), in ^{92}Zr well. Again, these data support the weak-coupling nature of these states [40,42]. However, the preceding arguments are not consistent with the results from Kent *et al.* in the positive-parity structure, where inelastic proton-scattering studies through isobaric analog resonances in ^{94}Mo did not support the weak coupling in ^{93}Nb [43].

B. $\pi 2p_{1/2}^{-1} \otimes (2_1^+, {}^{94}\mathrm{Mo})$ configuration

Low-lying negative-parity states in ^{93}Nb can be regarded as resulting from the $\pi 2p_{1/2}^{-1} \otimes (2_1^+, {}^{94}\mathrm{Mo})$ coupling. A doublet of negative-parity states ($J^\pi = 3/2_1^-$ at 687.4 keV and $J^\pi = 5/2_1^-$ at 810.7 keV) built on the $J^\pi = 1/2_1^-$ state confirms this assignment. Recently, we have studied excited states built on this doublet and identified *IV* excitations that correspond to the $2_{1,IV}^+$ states found in neighboring even-even nuclei [20]. Identifications are based on $M1$ and $E2$ strengths, energy systematics, and spin-parity assignments and from the comparison with *SM* calculations with the low-momentum nucleon-nucleon interaction $V_{\mathrm{low}\,k}$ [22]. Similar investigations will be provided in this paper for the *IS* negative-parity excitations, where seven states are expected to occur from the particle-core weak-coupling model (i.e., in addition to the $1/2_1^-$ single-particle state, the $3/2_1^-$ and $5/2_1^-$ states for the one-phonon excitations, and the $1/2_2^-$, $3/2_2^-$, $5/2_2^-$, $7/2_1^-$, and $9/2_1^-$ states for the two-phonon excitations).

C. Positive-parity states

Five new levels and 40 additional γ-ray transitions have been identified in this work. Table I lists the positive-parity states below 2.2 MeV, together with the γ rays that depopulate them. The decay properties evince a complex structure of levels, which decay to either the ground state or the lowest *IS* excitations. Despite possible admixtures of *IS* and *IV* wave functions in the odd-mass case, corresponding *MS* decay signatures might be expected analogous to those observed in the even-A $N = 52$ isotones [44,45]. From strong $M1$ transitions to the *IS* states and weakly collective $E2$ transitions to the ground state, we propose four candidates for *IV* excitations (i.e., the $9/2_3^+$, $5/2_2^+$, $7/2_3^+$, and $11/2_2^+$ levels at 1297.4, 1315.7, 1483.6, and 1603.5 keV, respectively). We propose them to be members of the quintet of *IV* excitations ($5/2_{IV}^+$, $7/2_{IV}^+$, $9/2_{IV}^+$, $11/2_{IV}^+$, and $13/2_{IV}^+$), which arise from the $\pi 1g_{9/2} \otimes (2_{1,IV}^+, {}^{92}\mathrm{Zr})$ coupling. From enhanced $B(E2)$ values to the $9/2_{IV}^+$ state, we propose the $11/2_3^+$ level at 1910.6 keV as a fragment of the two-phonon *MS* state. Additional details are provided as follows. However, these assignments are tentative because of the possibility for intermediate coupling and enhanced spin contributions from the unpaired proton to the $\hat{M}1$ operator. In fact, *SM* calculations show that $\approx 50\%$ of the $B(M1)$ strength arises from orbital contributions. The combined information of experiment and theory support the previous assignment of *IV* excitations and is discussed in Sec. IV.

1. 1297.4-keV $9/2_{IV}^+$ state

The 1297.4-keV level has been firmly assigned as $J^\pi = 9/2_3^+$ from the analysis of the angular correlation of the decay branches (see Table I and the bottom panel of Fig. 1). A mean lifetime of 380_{-75}^{+110} fs has been determined for this level from the Doppler-shift attenuation data. This value is in agreement with, but more accurate than, the 300_{-100}^{+300}-fs lifetime measured in a previous work [46]. Hence, the 553.1- and 318.3-keV transitions have $B(M1)$ values of 0.33(5) and $< 0.9\mu_N^2$, respectively. This level also decays with a small $E2$ strength to the ground state $B(E2; 9/2_{IV}^+ \rightarrow 9/2_1^+) = 1.2(2)$ W.u.. Both features are typical signatures for *MS* states.

2. 1315.7-keV $5/2_{IV}^+$ state

A $J^\pi = 5/2_2^+$ assignment has been given to this level from the angular correlation of the decay branches (see Table I) together with a mean lifetime of 530_{-170}^{+450} fs from the Doppler-shift attenuation data. The 571.5-keV transition to the $7/2_1^+$ state has a large $B(M1)$ value of $0.45(25)\mu_N^2$; nonetheless, the 506.7-keV transition to the $5/2_1^+$ state presents a large $B(E2)$ value. Hence, the excitation does not have a pure *IV* character, and intermediate coupling may mix *IS* and *IV* states.

3. 1483.6-keV $7/2_{IV}^+$ state

The 1483.6-keV level was previously assigned as $J^\pi = (7/2^+, 9/2^+)$. The angular-correlation analysis of the branches depopulating this state (see Table I) has firmly assigned it as $J^\pi = 7/2_3^+$. A short mean lifetime of 65(5) fs has been determined for the first time. The 674.8- and 400.8-keV transitions have large $B(M1)$ values of 0.58(6) and $< 0.7\mu_N^2$, respectively. The level decays to the ground state through a weakly collective $E2$ transition $B(E2) = 0.9(6)$ W.u.. Again, we find the characteristic features of an *MS* state.

4. 1603.5-keV $11/2_{IV}^+$ state

This level was previously assigned as $J^\pi = (11/2^+, 13/2^+)$. Here, we firmly assign it as $J^\pi = 11/2_2^+$ from the angular-correlation analysis of γ-ray branches and its decay to the $7/2_1^+$ state. A mean lifetime of $\tau = 465_{-125}^{+250}$ fs has been determined for the first time. This level has large $M1$ strengths to the one-phonon states and a large $B(E2; 11/2_2^+ \rightarrow 7/2_1^+) = 17(7)$ W.u.. Although the former suggests its *IV* character, the latter indicates admixtures of *IS* and *IV* wave functions (see Sec. IV on positive-parity states).

5. 1910.6-keV $11/2_{2,IV}^+$ state

The 1910.6-keV level has been assigned as $J^\pi = 11/2_3^+$, in disagreement with previous work, where $J^\pi = 7/2^{(+)}$ was proposed [47]. A lifetime of 200_{-30}^{+40} fs has been determined for this level, which decays with a weakly collective $B(E2)$ value of 5(2) W.u. to the proposed 1297.4-keV *IV* excitation. From this $B(E2)$ value and the spin assignment of the state,

TABLE I. Properties of low-lying positive-parity states in ^{93}Nb below 2.2 MeV. Excitation energies, spins, lifetimes, γ-ray energies, branching and mixing ratios, initial and final spins of the states, and reduced transition probabilities are listed. Asterisks indicate newly identified levels and γ-ray transitions. Uncertainties in the energies are 0.2 keV. Shell-model $B(M1)$ in μ_N^2 and $B(E2)$ values in W.u. calculated in this paper for relevant transitions are given in the rightmost two columns.

E_{level} (keV)	τ (fs)	$J_i^\pi \rightarrow J_f^\pi$	E_γ (keV)	I_γ	δ	$B(M1)$ (μ_N^2)	$B(E2)$ (W.u.)	$B(M1)$ [Shell model]	$B(E2)$
0.0	Stable								
744.0		$7/2_1^+ \rightarrow 9/2_1^+$	744.0	100	0.26(8)			0.095 91	7.836
809.1		$5/2_1^+ \rightarrow 7/2_1^+$	65.0	<1	$(M1/E2)$			0.1023	3.80
		$\rightarrow 9/2_1^+$	808.6	100(2)	$E2$			–	11.313
949.8		$13/2_1^+ \rightarrow 9/2_1^+$	949.8	100	$E2$			–	8.050
979.6	715^{+350}_{-180}	$11/2_1^+ \rightarrow 9/2_1^+$	978.8	100	−0.13(7)			0.043 28	5.761
1082.6	>1245	$9/2_2^+ \rightarrow 11/2_1^+$	103.7*	3(2)	$M1/E2$			1.747	1.091
		$\rightarrow 7/2_1^+$	338.6	100(2)	−0.09(2)			0.1795	2.299
		$\rightarrow 9/2_1^+$	1082.6	38(2)	$M1/E2$			0.007 31	3.992
1127.0^{IS}		$7/2_2^+ \rightarrow 5/2_1^+$	318.3	100(2)	−0.20(6)			0.016	0.6033
1297.4^{IV}	380^{+110}_{-75}	$9/2_3^+ \rightarrow 11/2_1^+$	318.3	31(5)	$(M1/E2)$	<0.9		0.021 85	1.420
		$\rightarrow 7/2_1^+$	553.1	61(5)	0.02(3)	0.33(5)	0.6(1)	0.2476	2.299
		$\rightarrow 9/2_1^+$	1297.4	100(5)	0.31(9)	0.04(1)	1.2(2)	0.003 66	0.0591
1315.7^{IV}	530^{+450}_{-170}	$5/2_2^+ \rightarrow 5/2_1^+$	506.7	24(4)	−1.4(8)	0.05(4)	235^{+300}_{-200}	0.190	0.3816
		$\rightarrow 7/2_1^+$	571.5	100(4)	0.14(4)	0.45(25)	15(10)	0.4072	3.864
1334.9^{IS}		$17/2_1^+ \rightarrow 13/2_1^+$	385.1	100(2)	$E2$				
1483.6^{IV}	65(5)	$7/2_3^+ \rightarrow 9/2_2^+$	400.8*	7(2)	$(M1/E2)$	<0.7		0.3459	0.02121
		$\rightarrow 5/2_1^+$	674.8	27(2)	−0.11(8)	0.58(6)	9(1)	0.1970	0.1264
		$\rightarrow 9/2_1^+$	1483.8	100(2)	−0.13(7)	0.20(2)	0.9(6)	0.004 22	5.568
1490.9^{IS}	>750	$15/2_1^+ \rightarrow 17/2_1^+$	156.0	14(2)	$(M1/E2)$	<0.04			
		$\rightarrow 13/2_1^+$	541.1	100(2)	−0.11(2)	<0.47	<12		
1603.5^{IV}	465^{+250}_{-125}	$11/2_2^+ \rightarrow 9/2_2^+$	520.9	13(3)	−0.07(9)	0.05(3)	0.6(4)	0.036 69	1.505
		$\rightarrow 11/2_1^+$	624.4	32(3)	0.11(6)	0.08(3)	1.5(6)	0.050 17	0.6245
		$\rightarrow 13/2_1^+$	653.6	100(3)	0.17(3)	0.22(9)	8(3)	0.1282	0.6027
		$\rightarrow 7/2_1^+$	859.5	22(3)		–	17(7)	–	2.817
		$\rightarrow 9/2_1^+$	1603.5	23(3)	$(M1/E2)$	<0.1	<1	0.005 66	0.053 78
1665.6^{IS}	350^{+100}_{-65}	$5/2_3^+ \rightarrow 5/2_1^+$	856.9	<1	$(M1/E2)$	<0.01		0.1079	0.3015
		$\rightarrow 7/2_1^+$	921.6	100(2)	1.4(2)	0.07(2)	90(35)	0.0740	2.891
		$\rightarrow 9/2_1^+$	1665.7*	2(2)	$E2$	–	<1	–	3.771
1679.8^{IS}	315^{+85}_{-60}	$7/2_4^+ \rightarrow 5/2_2^+$	364.1	60(3)	−0.17(9)	1.0(2)	130(50)	0.004 60	1.204
		$\rightarrow 9/2_3^+$	382.4	16(3)	$(M1/E2)$	<0.25		0.000 01	1.150
		$\rightarrow 5/2_1^+$	870.1*	7(3)	$(M1/E2)$	<0.01		0.006 50	1.995
		$\rightarrow 7/2_1^+$	935.7	100(3)	0.09(9)	0.10(2)	0.5(1)	0.000 23	2.452
		$\rightarrow 9/2_1^+$	1679.7	36(3)	$(M1/E2)$	<0.01		0.002 44	0.4702
1683.3	150^{+25}_{-20}	$9/2_4^+ \rightarrow 9/2_2^+$	600.7*	17(4)	$(M1/E2)$	<0.15		0.0117	0.012 88
		$\rightarrow 11/2_1^+$	704.2	42(4)	0.21(4)	0.20(4)	10(2))	0.054 73	0.046 24
		$\rightarrow 7/2_1^+$	939.3	100(4)	−0.20(4)	0.21(3)	5.4(8)	0.0962	0.6608
		$\rightarrow 9/2_1^+$	1683.2	54(4)	−0.34(25)	0.02(1)	1(1)	0.004 96	0.2582
1686.3	250^{+60}_{-40}	$13/2_2^+ \rightarrow 11/2_1^+$	707.4*	88(4)	−0.09(3)	0.20(5)	1.9(4)	0.012 21	1.480
		$\rightarrow 13/2_1^+$	736.5	90(4)	−0.27(13)	0.17(4)	13(3)	0.042 17	0.066 88
		$\rightarrow 9/2_1^+$	1686.3	100(4)	$E2$	–	3(1)	–	0.1624
1703.5^{IS}	220^{+280}_{-90}	$3/2_1^+ \rightarrow 5/2_2^+$	387.9*	100(4)	−0.02(6)	2.4(2.0)	4(3)	0.027 40	4.030
		$\rightarrow 5/2_1^+$	894.8*	87(4)	−0.3(1)	0.15(12)	10(6)	0.5956	5.015
1773.1^{IS}	125^{+20}_{-15}	$(1/2_1^+) \rightarrow 7/2_2^+$	646.0*	86(4)	$E2$			–	12.36
		$\rightarrow 5/2_1^+$	964.0	100(4)	$E2$			–	5.126

TABLE I. (*Continued.*)

E_{level} (keV)	τ (fs)	$J_i^\pi \rightarrow J_f^\pi$	E_γ (keV)	I_γ	δ	$B(M1)$ (μ_N^2)	$B(E2)$ (W.u.)	$B(M1)$ [Shell model]	$B(E2)$
1812.2	150^{+50}_{-35}	$(19/2^+) \rightarrow 17/2^+_1$	477.3	100					
1910.6^{IV}	200^{+40}_{-30}	$11/2^+_3 \rightarrow 9/2^+_3$	613.4*	10(6)	−0.20(12)	0.08(3)	5(2)	0.000 11	0.1171
		$\rightarrow 9/2^+_2$	828.1*	7(6)	−0.61(17)	0.02(1)	6(3)	0.040 79	3.748
		$\rightarrow 9/2^+_1$	1910.6	100(6)	$(M1/E2)$	<0.03		0.000 32	2.444
1916.1^{IV}	90(10)	$7/2^+_5 \rightarrow 5/2^+_2$	600.4*	36(4)	0.06(4)	0.66(10)	4(1)		
		$\rightarrow 9/2^+_2$	833.4	100(4)	−0.01(2)	0.69(10)	0.1(1)		
		$\rightarrow 5/2^+_1$	1107.2*	4(4)	$(M1/E2)$	<0.01			
		$\rightarrow 7/2^+_1$	1172.1*	12(4)	$(M1/E2)$	<0.03			
		$\rightarrow 9/2^+_1$	1915.5*	5(4)	$(M1/E2)$	<0.01			
1949.6^{IS}	770^{+1650}_{-320}	$7/2^+_5 \rightarrow 7/2^+_4$	270.1*	100(5)	$M1/E2$				
		$\rightarrow 9/2^+_2$	866.8*	9(5)	$M1/E2$				
		$\rightarrow 11/2^+_1$	971.1*	<2	$E2$				
		$\rightarrow 5/2^+_1$	1140.8	100(5)	0.21(5)				
		$\rightarrow 7/2^+_1$	1205.9	92(5)	$M1/E2$				
1949.7*	925^{+3700}_{-425}	$(7/2^+) \rightarrow 9/2^+_4$	266.4*	26(4)	$(M1/E2)$				
		$\rightarrow 11/2^+_2$	346.4*	41(4)	$E2$				
		$\rightarrow 9/2^+_1$	1949.8	82(4)	$(M1/E2)$				
1968.3		$(11/2^+, 13/2^+) \rightarrow 11/2^+_2$	365.0*	45(3)	$(M1/E2)$				
		$\rightarrow 15/2^+_1$	477.3	100(3)	$(M1/E2)$				
1968.8^{IS}	160^{+35}_{-30}	$11/2^+_3 \rightarrow 13/2^+_2$	282.5	27(5)	$(M1/E2)$	<1.5			
		$\rightarrow 9/2^+_4$	285.6	34(5)	$(M1/E2)$	<1.8			
		$\rightarrow 11/2^+_1$	990.0	64(5)	−0.83(16)	0.05(2)	20(7)		
		$\rightarrow 13/2^+_1$	1019.0	38(5)	−0.28(7)	0.04(1)	2(1)		
		$\rightarrow 7/2^+_1$	1225.0*	12(5)	$E2$		3(2)		
		$\rightarrow 9/2^+_1$	1968.9	100(5)	$(M1/E2)$	<0.2			
2002.5^{IS}	> 800	$11/2^+_4 \rightarrow 11/2^+_2$	399.1*	20(2)	$(M1/E2)$				
		$\rightarrow 9/2^-_1$	502.4*	12(2)	$E2$				
		$\rightarrow 15/2^+_1$	511.5*	<2	$E2$				
		$\rightarrow 11/2^+_1$	1023.7*	10(2)	$M1/E2$				
		$\rightarrow 13/2^+_1$	1052.8	100(2)	−0.63(7)				
$2122.6^{*,IS}$	115^{+30}_{-20}	$9/2^+_5 \rightarrow 7/2^+_3$	639.0*	36(3)	$(M1/E2)$	<0.2		0.095 35	0.0023
		$\rightarrow 11/2^+_1$	1143.7*	71(3)	$3.8^{+1.9}_{-1.0}$	0.01(1)	29(6)	0.036 91	2.275
		$\rightarrow 7/2^+_1$	1378.9*	29(3)	−1.9(8)	0.02(1)	0.2(2)	0.002 99	0.1651
		$\rightarrow 9/2^+_1$	2122.6*	100(3)	$(M1/E2)$	<0.02		0.000 78	1.508
2162.6^{IS}	410^{+300}_{-125}	$(13/2^+) \rightarrow 15/2^+_1$	671.7*	25(4)	$(M1/E2)$				
		$\rightarrow 11/2^+_1$	1183.7	100(4)	$(M1/E2)$				
		$\rightarrow 13/2^+_1$	1212.8*	61(4)	$(M1/E2)$				
2170.4^{IS}	350^{+165}_{-90}	$9/2^+_6 \rightarrow 9/2^+_2$	1087.6*	10(3)	$(M1/E2)$				
		$\rightarrow 11/2^+_1$	1192.5	100(3)	$(M1/E2)$				
		$\rightarrow 13/2^+_1$	1221.6	60(3)	$E2$				
		$\rightarrow 5/2^+_1$	1361.1*	31(3)	$E2$				
		$\rightarrow 7/2^+_1$	1426.1*	27(3)	$(M1/E2)$				
2184.0*	110^{+45}_{-30}	$(19/2^+) \rightarrow 17/2^+_1$	849.1*	100(2)	$(M1/E2)$				

we tentatively propose the 1910.6-keV level as a fragment of a two-phonon MS state (or second-order IV excitation) identified in the even-even neighbors. Arguments against this assignment are that neither the 1910.6-keV transition to the ground state nor the 828.1-keV γ-ray transition to the $9/2^+_2$ state have the enhanced $B(M1)$ character expected for an IV excitation, and the two-phonon MS state is generally identified at about 3 MeV. Nevertheless, the IV assignment is plausible,

since large fragmentation of the scissors-mode strength has been observed in the 2- to 4-MeV energy range in systematic studies of odd-A rare-earth nuclei [12,13,48].

6. 1968.8-keV $11/2^+_{IS}$ state

Although the spin and parity were assigned as $J^\pi = 11/2^+_3$ and we have a newly determined lifetime of 160^{+35}_{-30} fs for this state, only upper values for the $M1$ strengths of some of the transitions could be determined. The large $B(E2) = 20(7)$ W.u. observed for the 990.0-keV transition to the $11/2^+_1$ *IS* excitation is noteworthy.

7. 2122.6-keV $9/2^+_{IS}$ state

With an assigned $J^\pi = 9/2^+_5$ and a lifetime of 115^{+30}_{-20} fs, this state presents small $B(M1)$ values ($< 0.2\mu_N^2$) and a relatively large $B(E2) = 29(6)$ W.u. for the $11/2^+_1$ *IS* excitation.

D. Negative-parity states

Although some relevant information concerning the negative-parity states in ^{93}Nb has already been published [20], we present additional data collected in our measurements. Table II lists the results for levels up to 2.2 MeV.

1. 1284.8-keV $5/2^-_{IS}$ state

The 1284.8-keV level has been assigned as $J^\pi = 5/2^-_2$. A lifetime of 250^{+80}_{-50} fs has been measured for this level, which decays through a large $B(E2)$ value of 32^{+10}_{-9} W.u. to the $1/2^-_1$ single-particle state, which indicates a strong correlation between the wave functions of these states.

2. 1370.1-keV $5/2^-_3$ state

The 1370.1-keV level has been assigned as $J^\pi = 5/2^-_3$. A lower limit for the lifetime of > 790 fs has been determined for this level, which gives upper limits for the $B(E2)$ values to the $3/2^-_1$ and $5/2^-_1$ one-phonon states of < 7 and < 54 W.u., respectively. No decay to the ground state has been observed.

3. 1395.8-keV $7/2^-_{IS}$ state

The 1395.8-keV level has been assigned as $J^\pi = 7/2^-_1$. A lower limit for the lifetime of > 790 fs has been determined for this level, which gives upper limits for the $B(E2)$ values to the $3/2^-_1$ and $5/2^-_1$ states of < 18 and < 5 W.u., respectively. No decay for the ground state has been observed, which supports its *IS* character. In addition, the strong *IS* character of the transitions to the one-phonon states, listed in the last two columns of Table II, supports its *IS* assignment.

4. 1500.0-keV $9/2^-_{IS}$ state

This state was previously assigned as $J^\pi = 7/2^{(-)}$ [47]. Nevertheless, a $J^\pi = 9/2^-_1$ assignment is a better solution from the angular-correlation data. It also presents the longest lifetime, a newly measured 1170(300) fs, with respect to the other levels discussed in this section. An enhanced $B(E2)$ value of 27^{+15}_{-9} W.u. for the 689.6-keV $E2$ transition to the $5/2^-_1$ one-phonon state suggests this state as a member of the negative-parity *IS* coupling excitations. This large $B(E2)$ value is also predicted by our *SM* calculations, together with the *IS* character of the transition to the one-phonon states.

5. 1572.1-keV $3/2^-_{IS}$ state

A lifetime of 280^{+210}_{-100} fs has been determined for this $J^\pi = 3/2^-_2$ state, which gives large $B(E2)$ values to the $3/2^-_1$ and $5/2^-_1$ one-phonon states of 36^{+27}_{-19} and 21^{+12}_{-10} W.u., respectively. These large $B(E2)$ values support the *IS* character of the state. Decay to the ground state has not been observed. The strong $E2$ transitions to the one-phonon states confirm the *IS* character.

6. 1588.4-keV $5/2^-_{IS}$ state

A lower limit for the lifetime of > 1260 fs has been determined for this $5/2^-_4$ level, which gives upper limits for the $B(E2)$ values to the $3/2^-_1$ and $5/2^-_1$ one-phonon states of < 8 and < 13 W.u., respectively. Although the experimental data are not conclusive, our *SM* calculations predict relatively strong transitions and *IS* character for the transitions to the one-phonon states.

7. 1779.7-keV $5/2^-_{IV}$ state

Although the identification of *MS* states has already been discussed in Ref. [20], we include it for completeness. The previously proposed $(5/2^-)$ level at 1779.7 keV yields a new 1092-keV branch to the first $3/2^-_1$ excited state that has been revealed from the excitation function and coincidence data. The level has been assigned as $J^\pi = 5/2^{(-)}_5$ by the analysis of the angular-correlation data, and a mean lifetime of 105^{+43}_{-28} fs has been determined [20]. The 969- and 1092-keV transitions, which depopulate this state to the $2p^{-1}_{1/2} \otimes 2^+$ symmetric one-phonon states provide branching ratios of 100(5) and 8(5), respectively, and mixing ratios δ of 0.04(6) and 0.05(9), respectively. Hence, the 969-keV transition to the $5/2^-_1$ state has a large $B(M1)$ value of $0.55^{+0.24}_{-0.18}\mu_N^2$ and a small $B(E2)$ value of 0.5(2) W.u., while the 1092-keV transition to the $3/2^-_1$ state exhibits a much weaker $B(M1)$ strength of $0.03^{+0.04}_{-0.02}\mu_N^2$ and a $B(E2)$ value of $0.04^{+0.04}_{-0.03}$ W.u.. A large $B(M1)$ value for the $5/2^-_1$ one-phonon state was predicted, together with a strong *IV* character for such a transition.

8. 1840.6-keV $3/2^-_{IV}$ state

The 1840.6-keV level has been placed from our measurements. The angular-correlation analysis of the competing branches, which depopulate this state (see Table II) leads equally to either $J^\pi = 3/2^-$ or $5/2^-$ assignments. A mean lifetime of 103^{+35}_{-24} fs has been measured for this state, which yields large $B(M1)$ values of $0.29(8)\mu_N^2$ ($J^\pi = 3/2^-$) or $0.28(9)\mu_N^2$ ($J^\pi = 5/2^-$) for the 1153-keV transition. We propose, however, that this state is $3/2^-_3$, based on its proximity to the 1779.7-keV level and its rather different decay strengths.

TABLE II. Properties of low-lying negative-parity states in ^{93}Nb up to 2.1 MeV. Level and γ-ray energies, branching and mixing ratios, initial and final spins of the states, lifetimes, and reduced transition probabilities are listed. Asterisks indicate newly identified levels and γ-ray transitions. Uncertainties in the energies are 0.2 keV. Shell-model $B(M1)$ and $B(E2)$ predictions for relevant transitions as well as isoscalar (*IS*) and isovector (*IV*) components of the $E2$ operator are given in the rightmost four columns.

E_L (keV)	τ (fs)	$J_i^\pi \rightarrow J_f^\pi$	E_γ (keV)	I_γ	δ	$B(M1)$ (μ_N^2)	$B(E2)$ (W.u.)	$B(M1)$	$B(E2)$	*IS*	*IV*
30.9		$1/2_1^- \rightarrow 9/2_1^+$			$M4$						
687.4	400^{+70}_{-20}[a]	$3/2_1^- \rightarrow 1/2_1^-$	655.9	100	$(M1/E2)$						
810.7		$5/2_1^- \rightarrow 1/2_1^-$	779.6	100	$E2$						
		$\rightarrow 3/2_1^-$	123.3*	<1	$(M1/E2)$						
1284.8^{IS}	250^{+80}_{-50}	$5/2_2^- \rightarrow 1/2_1^-$	1253.5	100(4)	$E2$		32^{+10}_{-9}	–	–	–	–
		$\rightarrow 3/2_1^-$	597.3*	25(4)	0.14(4)	$0.20^{+0.10}_{-0.08}$	6^{+3}_{-2}	–	–	–	–
		$\rightarrow 5/2_1^-$	473.9*	5(4)	$(M1)$	<0.08		–	–	–	–
1370.1	>790	$5/2_3^- \rightarrow 3/2_1^-$	683.2*	30(4)	−0.34(5)	<0.05	<7	–	–	–	–
		$\rightarrow 5/2_1^-$	559.4	100(4)	−0.32(7)	<0.29	<54	–	–	–	–
1395.8^{IS}	>790	$7/2_1^- \rightarrow 3/2_1^-$	708.6	9(4)	$E2$		<18	–	8.50	28.61	−13.85
		$\rightarrow 5/2_1^-$	585.1	100(4)	−0.10(2)	<0.31	<5.2	0.000 03	0.879	9.17	−4.39
1500.0^{IS}	1170(300)	$9/2_1^- \rightarrow 5/2_1^-$	689.5(1)	18(3)	$E2$		27^{+15}_{-9}	–	10.63	35.39	−15.21
1572.1^{IS}	280^{+210}_{-100}	$3/2_2^- \rightarrow 3/2_1^-$	885.1*	37(5)	−1.60(14)	0.02(1)	36^{+27}_{-19}	0.002	14.46	25.71	−8.85
		$\rightarrow 5/2_1^-$	761.4*	100(5)	−0.28(3)	$0.27^{+0.16}_{-0.12}$	21^{+12}_{-10}	0.000 01	6.0	16.66	−6.44
		$\rightarrow 5/2_2^-$	287.4*	20(5)	$(M1)$	<1.09					
1588.4^{IS*}	>1260	$5/2_4^- \rightarrow 3/2_1^-$	901.2*	100(8)	−0.53(6)	<0.04	<8	0.0012	4.36	17.18	−5.26
		$\rightarrow 5/2_1^-$	777.8*	18(8)	$-4.03^{+1.32}_{-3.45}$	<0.001	<13	0.0069	16.94	34.19	−12.37
1779.7^{IV}	105^{+43}_{-28}	$5/2_5^- \rightarrow 3/2_1^-$	1092.4*	8(5)	0.05(9)	$0.03^{+0.04}_{-0.02}$	$0.04^{+0.04}_{-0.03}$	0.037	0.306	−0.74	2.35
		$\rightarrow 5/2_1^-$	969.0	100(5)	0.04(6)	$0.55^{+0.24}_{-0.18}$	0.5(2)	0.616	0.0001	−0.72	4.92
		$\rightarrow 1/2_{gs}^-$						—	4.28	12.63	19.87
1840.6^{IV*}	103^{+35}_{-24}	$3/2_3^- \rightarrow 3/2_1^-$	1153.4*	100(4)	0.14(4), 0.26(6)	0.28(9)	2.5(7), 8(2)	0.462	0.306	−4.36	4.90
		$\rightarrow 5/2_1^-$	1029.6*	20(4)	0.32(6), 0.17(8)	0.08(3)	4(1), 1(1)	0.046	0.078	−1.91	2.63
		$\rightarrow 1/2_{gs}^-$						–	5.99	13.03	14.55
1948.1	230^{+133}_{-69}	$7/2_2^{(-)} \rightarrow 5/2_1^-$	1137.4	100	0.05(4)	0.17(7)	0.2(1)				
1997.6*	92^{+22}_{-17}	$5/2_6^- \rightarrow 3/2_1^-$	1310.2*	12(5)	−0.29(12)	0.03(2)	$0.8^{+0.6}_{-0.4}$				
		$\rightarrow 5/2_1^-$	1186.9*	100(5)	−0.31(11)	$0.30^{+0.09}_{-0.07}$	12^{+4}_{-3}				
2012.6*		$3/2_4^- \rightarrow 3/2_1^-$	1325.8*	100(5)	$4.47^{+1.53}_{-0.94}$						
		$\rightarrow 3/2_2^-$	440.4*	6(5)							
2024.4^{IS*}	78^{+41}_{-25}	$3/2_5^- \rightarrow 3/2_1^-$	1337.1*	100(3)	$-4.70^{+0.84}_{-1.28}$	0.01(1)	91^{+76}_{-53}				
		$\rightarrow 3/2_2^-$	452.1*	3(3)	$(M1)$	<0.23					
2099.6	133^{+62}_{-36}	$7/2_3^{(-)} \rightarrow 5/2_1^-$	1288.9*	46(7)	−0.05(5)	0.05(1)	$0.2^{+0.3}_{-0.1}$				
		$\rightarrow 7/2_1^-$	703.8	100(7)							
2127.1*	235^{+171}_{-109}	$\rightarrow 7/2_1^+$	1383.1*	13(4)							
		$\rightarrow 5/2_1^-$	1316.61*	10(4)							
		$\rightarrow 7/2_1^-$	731.3*	18(4)							
		$\rightarrow 9/2_1^-$	626.9*	100(4)							
2153.8*	115^{+28}_{-20}	$\rightarrow 1/2_1^-$	2122.8*	100							

[a]Lifetime taken from Ref. [49].

A large $B(M1)$ value, this time for the $3/2_1^-$ one-phonon state was predicted.

The $B(M1)$ values from the 1779.7-keV state for the $5/2_1^-$ level and from the proposed 1840.6-keV state for the $3/2_1^-$ level are greater than from any other negative-parity states that feed the symmetric one-phonon states. These observations, together with the appearance of these states in the expected energy range ($\sim$2 MeV), support their assignment as first-order *IV* excitations.

The increasing level density and stronger mixing above 1.9 MeV make the attempt to characterize other excitations unrewarding.

IV. DISCUSSION

A. Shell-model calculations

For the present paper, we solve the model-space Schrödinger equation $PH_{\rm eff}P\Psi = EP\Psi$, where $H_{\rm eff} = H_0 + V_{\rm eff}$ and $V_{\rm eff}$ is the *SM* effective interaction. To derive $V_{\rm eff}$, we use the model-space folded-diagram methods detailed in Ref. [50], where we have the explicit expansion for the effective interaction:

$$V_{\rm eff} = \hat{Q} - \hat{Q}' \int \hat{Q} + \hat{Q}' \int \hat{Q} \int \hat{Q} - \hat{Q}' \int \hat{Q} \int \hat{Q} \int \hat{Q} + \cdots . \quad (5)$$

In this series, $\hat{Q}$ represents the irreducible vertex function, which consists of irreducible valence-linked diagrams, and the integral sign denotes a generalized folding operation. In the $\hat{Q}$ box, we have included core-polarization diagrammatic contributions up to second order, which have been shown to be a good approximation to a nonperturbative all-order summation in the absence of $3N$ forces [51]. The intermediate particle and hole states are allowed two oscillator shells above and below the model space (which is discussed later). We sum the previous series by using the Lee-Suzuki iteration method [52].

By starting from any high-precision NN interaction V_{NN}, we can derive a resolution-dependent low-momentum interaction $V_{{\rm low}\,k}$, which preserves all low-energy data below the chosen momentum cutoff [22]. For this paper, we have used the CD-Bonn interaction as V_{NN} with a momentum-cutoff value of $\Lambda = 2.0$ fm. There have now been a number of nuclear structure studies that use this low-momentum NN interaction in this nuclear region to describe a variety of nuclei and their observables [20,53–55].

By following the prescription of Ref. [21], we choose to use ^{88}Sr as the inert core for these calculations. Valence neutrons can then occupy the following single-particle orbits above the $N = 50$ closed shell: $g_{7/2}$, $d_{5/2}$, $d_{3/2}$, $s_{1/2}$, and $h_{11/2}$. For the valence protons, we take the $p_{1/2}$ and $g_{9/2}$ orbits consistent with a $Z = 38$ proton core. The single-particle energies ϵ_j were obtained from the experimental values in the ^{89}Y and ^{89}Sr nuclei; for reference, they are listed in Table III. These single-particle energies differ slightly from those used in Ref. [20], which were tuned to best reproduce the experimental spectra in ^{90}Zr and ^{90}Sr. To keep the calculations as free from adjustable parameters as possible, we now use the experimental values, but our current results on the negative-parity states in ^{93}Nb are essentially unchanged from those reported earlier [20].

TABLE III. Single-particle energies for the orbits used in *SM* calculations.

Proton orbits:	$p_{1/2}$	$g_{9/2}$			
Energy (MeV)	−0.91	0.0			
Neutron orbits:	$g_{7/2}$	$d_{5/2}$	$d_{3/2}$	$s_{1/2}$	$h_{11/2}$
Energy (MeV)	1.47	0.0	2.01	1.03	3.00

To test this interaction, we have compared the calculated proton-proton (*pp*) and neutron-neutron (*nn*) spectra with the experimentally observed spectra for the ^{90}Sr and ^{90}Zr nuclei up to excitation energies of $\sim$3 MeV [56]. Here, we see there is generally fair agreement between the calculated and the experimental levels, by noting that the $V_{{\rm low}\,k}$ calculation gave rather similar results to those obtained in Ref. [21], in which the surface δ interaction, with tuned parameters, was used as the residual interaction. Particularly, Fig. 4 shows a partial-level scheme with first-order *IS* and *IV* positive-parity excitations identified in this paper compared with $V_{{\rm low}\,k}$ *SM* calculations. The calculations were carried out by using the OXBASH *SM* code [57] with a model-space file and a $V_{{\rm low}\,k}$ interaction file specifically generated, by using the foregoing single-particle energies, for use with this code.

For comparison with experimental work, we explicitly calculate the transition rates, defined as

$$B(M1; J_i \to J_f) = \frac{|\langle J_f \| M1 \| J_i \rangle|^2}{2J_i + 1}. \quad (6)$$

In these calculations, we have kept the bare-orbital g factors $g_\pi^l = 1\ \mu_N$ and $g_\nu^l = 0$, while we have used empirical values for the spin g factors $g_\pi^s = 3.18\ \mu_N$ and $g_\nu^s = -2.18\ \mu_N$. We note that these values for the spin g factors are not fit to any experimental data. Similarly, the $E2$ transition operator is

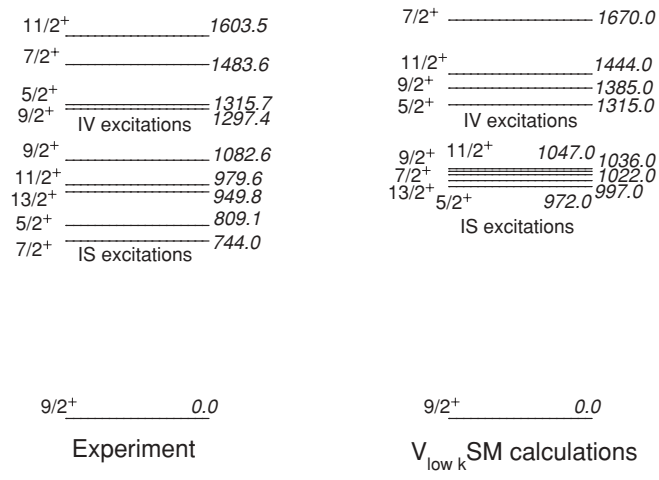

FIG. 4. ^{93}Nb partial-level scheme, which shows first-order *IS* and *IV* positive-parity excitations (left) as compared with $V_{{\rm low}\,k}$ *SM* calculations (right).

TABLE IV. Spin and orbital contributions to the large $M1$ transitions observed in the SM calculations. Values are given in units of μ_N^2.

J_i	$\rightarrow J_f$	Spin $B(M1)$	Orbital $B(M1)$
$5/2_2^+$	$\rightarrow 7/2_1^+$	0.1434	0.1280
$7/2_3^+$	$\rightarrow 9/2_1^+$	0.1248	0.09257
	$\rightarrow 5/2_1^+$	0.053 69	0.04515
$9/2_3^+$	$\rightarrow 7/2_1^+$	0.057 97	0.069 53
$11/2_2^+$	$\rightarrow 13/2_1^+$	0.039 41	0.035 86

given by

$$T(E2) = e_\pi \sum_{i=1}^{Z} r_i^2 Y_\mu^{(2)}(\hat{r}_i) + e_\nu \sum_{i=1}^{N} r_i^2 Y_\mu^{(2)}(\hat{r}_i), \qquad (7)$$

where e_π and e_ν are the proton and neutron effective charges. Here, we use the same effective charges as in Ref. [20]; that is, $e_\pi = 1.85e$ and $e_\nu = 1.30e$.

B. Positive-parity states

In even-even nuclei, the signature of large magnetic dipole transition strength from a proposed *IV* excitation to the *IS* state is typically sufficient for identification of MS states. Because of the presence of an unpaired nucleon in an odd-mass nucleus, however, further theoretical evidence is needed to confidently identify an MS state. Here, in addition to the magnetic dipole transition rates, we decompose the relevant transitions into their spin and orbital components to rule out large $M1$ strengths because of spin-flip transitions. The calculations are presented in Table IV, where we only have included the results for states in which a clearly analogous state was experimentally present.

1. *One-phonon IS excitations*

The lowest-lying quintet $\{5/2_1^+, 7/2_1^+, 9/2_2^+, 11/2_2^+, 13/2_2^+\}$ can clearly be identified as the coupling of the $g_{9/2}$ proton to the 2_1^+ state in ^{92}Zr. While the experiments were not sensitive to the ground-state decay rates of these states, the SM calculations reveal all to have collective $B(E2)$ transitions to the $9/2_1^+$ ground state, with predominantly *IS* character. Nonetheless, the proposed $9/2_2^+$ member of the quintet at 1082.6 keV decays preferentially to the $7/2_1^+$ state at 744.0 keV rather than by a 1082.6-keV transition to the ground state. Two-state mixing calculations between the 1082.6-keV and ground states were performed in an attempt to explain this anomalous decay [40], and the results are in agreement with decay strengths in neighboring ^{92}Mo and ^{94}Mo nuclei. Shell-model calculations yield a large $B(M1; 9/2_2^+ \rightarrow 7/2_1^+) = 0.18\mu_N^2$, which suggests mixing with the $9/2_3^+$ *IV* excitation at 1297.4 keV, only $\approx$200 keV above.

2. *One-phonon IV excitations*

We start with the 1279.4-keV $9/2_3^+$ state, which exhibits a strong $M1$ transition to the symmetric one-phonon $7/2_1^+$ state and a weakly collective $E2$ transition to the $9/2_1^+$ ground state experimentally. In the calculations, we find a qualitatively similar decay pattern, although the rates are slightly underpredicted in the SM calculations. In Table IV, we see that this magnetic dipole transition is almost equally composed of spin and orbital parts, as is typically seen in such transitions [20], which leads to a confident assignment as an MS excitation.

The 1483-keV $7/2_3^+$ state exhibits a similar experimental decay pattern, with strong $M1$ transitions to both the $9/2_2^+$ and the $5/2_1^+$ states (although only an upper bound is determined for the transition to the $9/2_2^+$ state) and a weak $E2$ transition to the ground state. In the SM calculations, the large $M1$ transitions are again in qualitative agreement with the experimental measurements. In the calculations, the transition to the ground state, however, is significantly more collective than the experimental value, but not inconsistent with its proposed identification as an MS excitation. To confirm this, we again turn to Table IV, where we see that, for both of these $M1$ transitions, there is significant orbital character, which indicates an MS state.

From an inspection of $M1$ transition strength, it appears that the 1315-keV $5/2_2^+$ state would be a reasonable *IV* excitation candidate with a strong transition to the $7/2_1^+$ state. This observation is coupled with a collective $E2$ transition to the same state, indicative of an *IS* transition. This is perhaps caused by the mixing between this state and the 1665.6-keV $5/2_3^+$ state, which also exhibits a weaker but sizable $M1$ transition to the $7/2_1^+$ state, as well as a collective $E2$ transition to the same state. The SM presents a picture consistent with this assessment, by predicting an additional magnetic dipole transition to the $5/2_1^+$ state, which is not seen experimentally. The MS character of these large $M1$ transitions can be confirmed in Table IV, where we see a sizable orbital component of the transitions.

Finally, a case can be made for proposing the 1603-keV $11/2_2^+$ state as a member of the *IV* quintet because of the experimentally observed $M1$ transition to the $13/2_1^+$ one-phonon symmetric state. This is borne out in the calculations, where we see the expected equal distribution of spin and orbital $M1$ transition strengths. Again, some mixing with higher *IS* excitations is likely manifested in the collective $E2$ transition to the one-phonon symmetric states seen experimentally, which are also apparent in the SM.

It would seem that a suitable candidate for the $13/2_2^+$ *IV* excitation is the 1686-keV state, with large $B(M1)$s to both the $11/2_1^+$ and the $13/2_1^+$ states observed experimentally. This, however, is unfortunately not apparent in the SM calculations as the $M1$ transitions predicted are too weak to support this identification.

V. CONCLUSION

In this paper, we have investigated *IV* and *IS* excitations in the positive- and negative-parity structures of ^{93}Nb. Identifications are based on $M1$ and $E2$ transition strengths, spin and parity assignments, and shell-model calculations. These findings support the weak-coupling picture of fermions and bosons in both $\pi 2p_{1/2}^{-1} \otimes {}^{94}$Mo and

$\pi 1g_{9/2} \otimes {}^{92}$Zr configurations. The marked separation of the positive- and negative-parity structures in ^{93}Nb facilitates the comprehension of such a relevant interaction, especially in the simpler scenario for the negative-parity states. Overall, larger $B(M1)$ values are observed in this nucleus as compared with the even-A neighbors as the result of additional spin-flip effects. Levels assigned as *IV* excitations lie at lower energies than that observed for the $2^+_{1,MS}$ state in ^{92}Zr (1.847 MeV). Interestingly, similar transition strengths of about 30 W.u. are found from the levels characterized as *IS* excitations.

ACKNOWLEDGMENTS

This work was supported by the US National Science Foundation under Grant No. PHY-0652415, the Deutsche Forschungsgemeinschaft, Grants No. Jo 391/3-1 and No. SFB 634, the Natural Sciences and Engineering Research Council (NSERC), and by the US Department of Energy under Grant No. DE-FG02-91ER40609 and DE-FC02-07ER41457 (UNEDF SciDAC Collaboration). TRIUMF receives federal funding via a contribution agreement through the National Research Council of Canada.

[1] K. Heyde and P. J. Brussaard, Nucl. Phys. A **104**, 81 (1967).
[2] A. Bohr and B. R. Mottelson, Mat. Fys. Medd. Dan. Vid. Selsk. **27**, 16 (1953).
[3] D. C. Choudhury, Mat. Fys. Medd. Dan. Vid. Selsk. **28**, 4 (1954).
[4] R. D. Lawson and J. L. Uretsky, Phys. Rev. **108**, 1300 (1957).
[5] A. de Shalit, Phys. Rev. **122**, 1530 (1961).
[6] R. E. Anderson, J. J. Kraushaar, I. C. Oelrich, R. M. DelVecchio, R. A. Naumann, E. R. Flynn, and C. E. Moss, Phys. Rev. C **15**, 123 (1977).
[7] I. C. Oelrich, K. Krien, R. M. DelVecchio, and R. A. Naumann, Phys. Rev. C **14**, 563 (1976).
[8] I. J. van Heerden and W. R. McMurray, Z. Phys. **260**, 9 (1973).
[9] B. Cheal *et al.*, Phys. Rev. Lett. **102**, 222501 (2009).
[10] N. Lo Iudice and F. Palumbo, Phys. Rev. Lett. **41**, 1532 (1978).
[11] I. Bauske *et al.*, Phys. Rev. Lett. **71**, 975 (1993).
[12] A. Nord *et al.*, Phys. Rev. C **54**, 2287 (1996).
[13] A. Nord *et al.*, Phys. Rev. C **67**, 034307 (2003).
[14] N. Huxel *et al.*, Nucl. Phys. A **645**, 239 (1999).
[15] N. Pietralla, P. von Brentano, and A. F. Lisetskiy, Prog. Part. Nucl. Phys. **60**, 225 (2008).
[16] N. Pietralla *et al.*, Phys. Rev. Lett. **83**, 1303 (1999).
[17] G. Rainovski, N. Pietralla, T. Ahn, C. J. Lister, R. V. F. Janssens, M. P. Carpenter, S. Zhu, and C. J. Barton III, Phys. Rev. Lett. **96**, 122501 (2006).
[18] O. Burda *et al.*, Phys. Rev. Lett. **99**, 092503 (2007).
[19] F. Iachello and A. Arima, *The Interacting Boson Model* (Cambridge University Press, Cambridge, UK, 1987).
[20] J. N. Orce *et al.*, Phys. Rev. Lett. **97**, 062504 (2006).
[21] A. F. Lisetskiy, N. Pietralla, C. Fransen, R. V. Jolos, and P. von Brentano, Nucl. Phys. A **677**, 100 (2000).
[22] S. K. Bogner, T. T. S. Kuo, and A. Schwenk, Phys. Rep. **386**, 1 (2003).
[23] M. T. McEllistrem, *Nuclear Research with Low Energy Accelerators* (Academic, New York, 1967), p. 167; P. E. Garrett, N. Warr, and S. W. Yates, J. Res. Natl. Inst. Stand. Technol. **105**, 141 (2000).
[24] T. Belgya, G. Molnár, and S. W. Yates, Nucl. Phys. A **607**, 43 (1996).
[25] A. E. Blaugrund, Nucl. Phys. **88**, 501 (1966).
[26] K. B. Winterbon, Nucl. Phys. A **246**, 293 (1975).
[27] C. A. McGrath, P. E. Garrett, M. F. Villani, and S. W. Yates, Nucl. Instrum. Methods A **421**, 458 (1999).
[28] A. Linnemann, Ph.D. thesis, IKP, University of Cologne, 2005 (unpublished).
[29] J. Eberth, H. G. Thomas, P. von Brentano, R. M. Lieder, H. M. Jäger, H. Kämmerfing, M. Berst, D. Gutknecht, and R. Henck, Nucl. Instrum. Methods A **369**, 135 (1996).
[30] H. J. Rose and B. M. Brink, Rev. Mod. Phys. **39**, 306 (1967).
[31] K. S. Krane and R. M. Steffen, Phys. Rev. C **2**, 724 (1970); K. S. Krane, R. M. Steffen, and R. M. Wheeler, At. Data Nucl. Data Tables **11**, 351 (1973).
[32] T. Kakavand and K. P. Singh, Acta Phys. Pol. B **33**, 737 (2002).
[33] [http://www.nndc.bnl.gov] (*NNDC database*).
[34] H. C. Sharma and N. Nath, Nucl. Phys. A **142**, 291 (1970).
[35] H. Göbel, E. J. Feicht, and H. Vonach, Z. Phys. **240**, 430 (1970).
[36] M. R. Cates, J. B. Ball, and E. Newman, Phys. Rev. **187**, 1682 (1969).
[37] C. Fransen, V. Werner, D. Bandyopadhyay, N. Boukharouba, S. R. Lesher, M. T. McEllistrem, J. Jolie, N. Pietralla, P. von Brentano, and S. W. Yates, Phys. Rev. C **71**, 054304 (2005).
[38] M. E. Bunker, B. J. Dropesky, J. D. Knight, and J. W. Starner, Phys. Rev. **127**, 844 (1962).
[39] Y. Yoshizawa, B. Herskind, and M. Hoshi, J. Phys. Soc. Jpn. **50**, 2151 (1981).
[40] M. Kregar and G. G. Seaman, Nucl. Phys. A **179**, 153 (1972).
[41] P. H. Stelson, R. L. Robinson, W. T. Milner, F. K. McGowan, and M. A. Ludington, Bull. Am. Phys. Soc. **16**, 619 (1971).
[42] K. Alder, A. Bohr, T. Huus, B. Mottelson, and A. Winther, Rev. Mod. Phys. **28**, 432 (1956).
[43] J. J. Kent, W. R. Coker, and C. E. Watson, Z. Phys. **256**, 199 (1972).
[44] C. Fransen *et al.*, Phys. Rev. C **67**, 024307 (2003).
[45] V. Werner *et al.*, Phys. Lett. B **550**, 140 (2002).
[46] I. K. Lemberg and A. A. Pasternak, Izv. Akad. Nauk SSSR, Ser. Fiz. **38**, 1600 (1974).
[47] V. D. Avchukhov, K. A. Baskova, V. A. Bondarenko, A. B. Vovk, L. I. Govor, and A. D. Demidov, Izv. Akad. Nauk SSSR, Ser. Fiz. **46**, 947 (1982).
[48] J. Enders, N. Huxel, P. von Neumann-Cosel, and A. Richter, Phys. Rev. Lett. **79**, 2010 (1997).
[49] C. M. Baglin, Nucl. Data Sheets **80**, 1 (1997).
[50] T. T. S. Kuo and E. Osnes, *Lecture Notes in Physics* (Springer-Verlag, New York, 1990), Vol. 364.
[51] J. D. Holt, J. W. Holt, T. T. S. Kuo, G. E. Brown, and S. K. Bogner, Phys. Rev. C **72**, 041304(R) (2005).
[52] S. Y. Lee and K. Suzuki, Phys. Lett. **91B**, 79 (1980); K. Suzuki and S. Y. Lee, Prog. Theor. Phys. **64**, 2091 (1980).
[53] J. D. Holt, N. Pietralla, J. W. Holt, T. T. S. Kuo, and G. Rainovski, Phys. Rev. C **76**, 034325 (2007).
[54] O. Burda *et al.*, Phys. Rev. Lett. **99**, 092503 (2007).
[55] V. Werner *et al.*, Phys. Rev. C **78**, 031301(R) (2008).
[56] J. D. Holt, N. Pietralla, J. W. Holt, and T. T. S. Kuo (unpublished).
[57] B. A. Brown, A. Etchegoyen, N. S. Godwin, W. D. M. Rae, W. A. Richter, W. E. Ormand, E. K. Warburton, J. S. Winfield, L. Zhao, and C. H. Zimmerman, MSU-NSCL Report Number 1289 (unpublished).